

TransfoREM: Transformer aided 3D Radio Environment Mapping

Gautham Reddy*, Ismail Güvenç*, Mihail L. Sichitiu*, Arupjyoti Bhuyan†, Bryton Petersen†
Jason Abrahamson†

*Department of Electrical and Computer Engineering, NC State University, Raleigh, NC 27606

†Idaho National Laboratory, Idaho Falls, ID 83415

Email: {greddy2, iguvenc, mlsichit}@ncsu.edu, {arupjyoti.bhuyan, Bryton.Petersen, jason.abrahamson}@inl.gov

Abstract—Providing reliable cellular connectivity to Unmanned Aerial Vehicles (UAV) is a key challenge, as existing terrestrial networks are deployed mainly for ground-level coverage. The cellular network coverage may be available for a limited range from the antenna side lobes, with poor connectivity further exacerbated by UAV flight dynamics. In this work, we propose TransfoREM, a 3D Radio Environment Map (REM) generation method that combines deterministic channel models and real-world data to map terrestrial network coverage at higher altitudes. At the core of our solution is a transformer model that translates radio propagation mapping into a sequence prediction task to construct REMs. Our results demonstrate that TransfoREM offers improved interpolation capability on real-world data compared against conventional Kriging and other machine learning (ML) techniques. Furthermore, TransfoREM is designed for holistic integration into cellular networks at the base station (BS) level, where it can build REMs, which can then be leveraged for enhanced resource allocation, interference management, and spatial spectrum utilization.

Index Terms—3D Radio Environment Maps, Transformers, Unmanned Aerial Vehicle.

I. INTRODUCTION

The traditional approach to wireless network planning has relied on deterministic propagation models. However, the future network landscape will be more dynamic, with complex interactions arising from extreme densification, support for a wider variety of applications, and the integration of new high-frequency bands. Such advances will present challenges in interference management, enhanced coverage, and energy utilization, necessitating more data-driven and real-time network management tools. To address these needs, future networks will benefit from the Radio Environment Map (REM) capability to proactively maintain a spatio-temporal database of the Radio Frequency (RF) environment in the network vicinity [3].

REMs serve as a comprehensive view of the network coverage over space, helping to solve key challenges such as:

- **Dynamic Spectrum Access:** Wireless spectrum is a valuable and increasingly scarce resource. Existing practices of fixed-spectrum allocation lead to under-utilization, creating scope for sharing based on regional usage. REMs

We use measurement data from prior published works [1], [2]. This research is supported in part by the NSF award CNS-2332835 and the INL Laboratory Directed Research Development (LDRD) Program under BMC No. 264247, Release No. 26 on BEA's Prime Contract No. DE-AC07-05ID14517. Corresponding author: Ismail Güvenç (email: iguvenc@ncsu.edu).

provide a solution to this problem by acting as spectrum usage mapping tools, allowing networks to identify and utilize underused frequency bands across space. This capability augments the Radio Dynamic Zone (RDZ) [1] concept being developed for new users to harmoniously share spectrum with incumbent users.

- **Serving Aerial Users:** Terrestrial cellular networks, designed for ground-level users, pose coverage challenges for high-altitude applications [4]. Aerial users have a clear line-of-sight (LOS) to multiple base station (BS)s simultaneously, but they also experience varying antenna patterns due to the downward tilt of terrestrial BSs. These effects lead to complicated coverage management and high-interference or weak signal zones in 3D space. Hence, a 3D REM helps to understand and better manage connectivity at higher altitudes.

REMs help wireless networks overcome these challenges, transforming them to optimize future performance proactively. The development of effective REM construction techniques, ranging from parametric models to deep learning-based spatial mapping [5], has been essential to achieve this goal. Toward this end, we introduce TransfoREM to estimate the radio propagation by modeling signal strength as sequences originating from the BS as seen in Fig. 1. This framework is specifically designed for deployment at individual BSs, where it can learn the local radio footprint to manage better connectivity, interference, and mobility within its coverage area. The main contributions of this work are as follows.

- 1) Radio propagation modeling is posed as a sequence estimation task in the spherical coordinate system, aligning with the nature of outward radiation and antenna directivity gains inherent to wireless signal propagation.
- 2) We show that a transformer model with masked sequence translation, a technique borrowed from language processing, can accurately predict radio propagation. This method is effective for mapping radio environments with limited real-world data.
- 3) Our approach demonstrates a true 3D REM generation framework that extrapolates from both 2D sample measurement planes and 3D spatial data, outperforming Kriging and machine learning (ML) techniques.

The rest of the paper is organized as follows. Section II

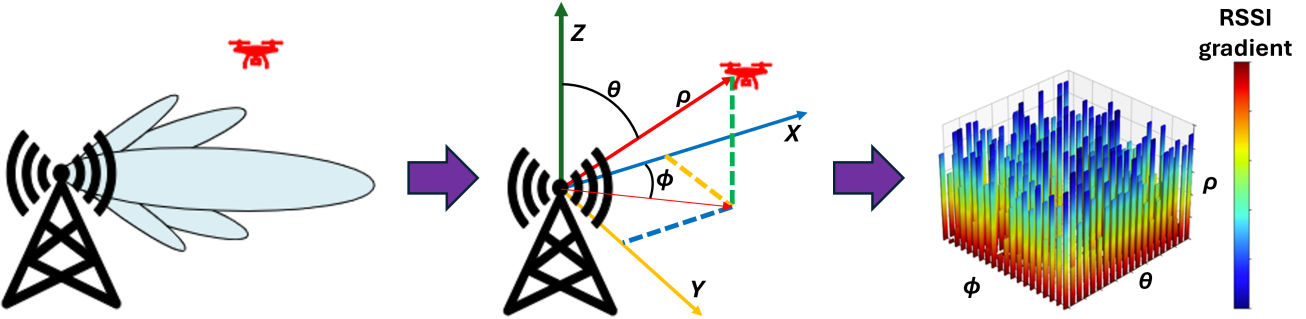


Fig. 1. The spherical coordinate system representation of a UAV position and its associated received signal strength indicator (RSSI) sequences in space.

provides a literature review of related work. Section III details the radio propagation system model, real-world data collection, and analysis. Section IV then discusses the transformer model used to generate REMs. In Section V, we present the experimental results, including comparative case studies using the data and results from [1], [2], [6]. Finally, Section VI concludes the article.

II. RELATED WORK

With REMs holding significant importance in wireless network planning and operation, they have been extensively studied using various reconstruction techniques. Broadly, these REM techniques can be categorized into model-driven methods, data-driven methods, and a hybrid of model- and data-driven methods [7]. The model-driven methods rely on path loss models, geometry-based ray tracing methods, and stochastic models that capture the behavior of received signal strength. However, such methods are limited by the practical deviations such as multi-path and diffraction effects in real-world.

Recent approaches, such as [8] have focused more on incorporating real-world data through data-driven REM mapping techniques. A major hurdle for these techniques, however, is the high sampling requirement, as both 2D and 3D REM reconstruction benefit from a dense sampling rate. Prior work has sought to address this by identifying and prioritizing specific spatial regions based on the environment's geometric and terrain information to focus data collection efforts [9], [10]. Recognizing the shortcomings of both stand-alone model and data-driven techniques, the hybrid (model + data-driven) REM approach offers a robust solution by complementing the advantages of each. In this work, we utilize this hybrid methodology to develop a REM framework designed for deployment at individual BS sites, enabling the learning of the unique local radio propagation environment.

Recent hybrid REM generation approaches include [11], where a graph attention network (GAT) is leveraged to fuse model-based spatio-spectral correlation with data-driven radiomap generation. Similarly, [12] employs a generative adversarial network (GAN) with unsupervised learning to build REMs from sparse signal strength measurements. Other notable methods include the triple-layer ML technique in [2],

which uses a stagewise process of linear regression, ensemble methods, and a Gaussian process regression (GPR) to predict and refine spatial radio Key Performance Indicators (KPIs) using real data. Furthermore, [13] introduces a transformer-based technique to learn spatial correlation trends, effectively mimicking the Kriging interpolation method without requiring a semi-variogram. While these methods are all novel in their approaches, our proposed work distinguishes itself as a truly physics-inspired technique that traces radio wave propagation by learning foundational model knowledge and then adapting according to measurement data.

III. SYSTEM MODEL AND DATA ANALYSIS

Wireless channel modeling is a widely researched area that serves as a fundamental step in system design and analysis. Spatial channel modeling is a subset of this effort, with standardization bodies such as 3rd Generation Partnership Project (3GPP) publishing detailed channel characteristic models that range from large-scale outdoor channels to indoor environmental channels. Generally, these statistical channel models do not accurately capture the site-specific channel behavior and need to be augmented with data-driven perception to improve connectivity management at individual BSs. To build this capability, we begin with a propagation channel model abstraction similar to the one presented in [14].

A. Deterministic Channel Propagation Model

For a user k connected to a BS b , the received signal strength $P_{b,k_{\text{dB}}}(\rho, \phi, \theta)$ as a function of radial separation ρ and 3D angles ϕ, θ according to Fig. 1, in dB-scale is defined as:

$$P_{b,k_{\text{dB}}}(\rho, \phi, \theta) = P_{b_{\text{dB}}} + G_{b,k_{\text{dB}}}(\rho, \phi, \theta) + N, \quad (1)$$

where $P_{b_{\text{dB}}}$ is the transmit power of BS b , $G_{b,k_{\text{dB}}}$ is the large scale channel loss model, and N is the Gaussian noise power. With $G_{b,k_{\text{dB}}}$ defined as,

$$G_{b,k_{\text{dB}}}(\rho, \phi, \theta) = \text{PL}_{\text{dB}}(\rho) + \text{SF}_{\text{dB}}(\rho, \phi, \theta) + A_{\text{dB}}(\phi, \theta), \quad (2)$$

where PL_{dB} is the path loss, SF_{dB} is the shadow fading, and A_{dB} is the antenna array gain. The path loss and shadow fading models vary depending on the environmental context, ranging from the simplistic free space path loss (FSPL) to the 3GPP

channel models defined in TR 38.901. These path loss models are generally coupled with shadow fading models that depend on LOS conditions and surrounding terrain information. The ideal antenna gain patterns can be characterized before deployment. However, actual beam patterns may deviate based on the surrounding reflections at the BS site.

Together, these effects are best studied in the spherical coordinate system originating from the BS. This outward radiation phenomenon, characterized by radial path loss attenuation and angular antenna beam pattern correlation, is captured in (2). The equation also features a shadow fading component with regional correlation properties that are better captured in the Cartesian coordinate system. These spatial correlation properties are crucial for interpolation in REM generation, and we quantify this understanding using the 3D signal strength dataset presented in [1].

B. Spatial Correlation Properties of 3D Signal Strength Data

The dataset presented in [1] comprises reference signal received power (RSRP) measurements from a BS collected at five distinct altitudes, spanning from 30 m to 110 m using an UAV at the Aerial Experimentation and Research Platform for Advanced Wireless (AERPAW) testbed. The authors used this dataset to conduct a correlation analysis of the shadowing component in received signals across space. Specifically, Sections VI-A and VI-B of their work detail a joint correlation equation for the shadowing component based on both horizontal and vertical separation distances between pairwise spatial points. However, rather than separating the contributions of path loss and shadowing, we investigate the correlation of total received signal strength values in 3D space, as follows:

- 1) We define a spherical grid system with azimuth and elevation angles binned at 0.1 radian increments. Measurement points at varying radii from each 3D angular bin are then grouped.
- 2) From each 3D angular bin group, we compute pairwise RSRP correlations and sort the resulting values based on their radial separation into bins of size 5 m.
- 3) The pairwise correlation values within each radial separation bin are then averaged across all 3D angular bins to derive a combined RSRP correlation plot as a function of radial separation distance.

We note that the correlation plot in Fig. 2 shows a strong correlation along the radial direction, extending up to a range of 100 m, whereas the shadow fading correlation behavior in [1] drops off at less than 50 m. This observation aligns with (2), reinforcing the need to interpolate radio signals in the spherical coordinate system while retaining a Cartesian view for shadow fading interpolation. This joint correlation analysis provides a comprehensive understanding of the spatial dependencies of radio signals, thus forming the basis of our proposed REM reconstruction technique.

IV. TRANSFOREM SYSTEM DESIGN

Recognizing the radial nature of radio wave propagation, we formulate the REM generation as a sequence estimation task

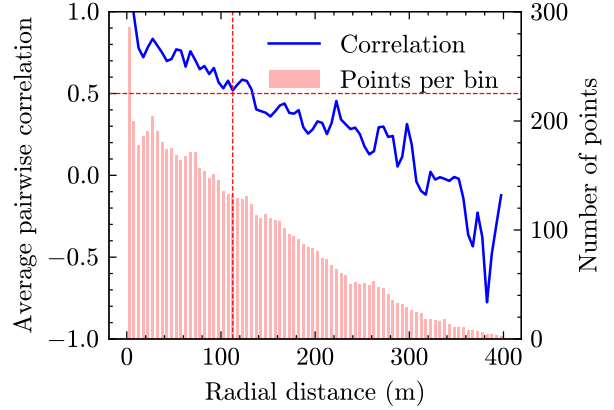


Fig. 2. Radial distance up to 100 m have correlation values greater than 0.5.

of varying signal strengths originating from the BS. Fig. 1 depicts the radio wave propagation to each point in space as a unique sequence. Leveraging the strong sequence predictive capabilities of Transformers, we develop the TransfoREM estimator. This estimator is initially trained on a deterministic model and then fine-tuned using real-world data to improve prediction accuracy.

A. Radio Environment Viewed in Spherical Coordinate System

Every 3D coordinate $[x, y, z]$ in space is transformed into the spherical coordinate system $[\rho, \phi, \theta]$, as seen in Fig. 1, using the formulae:

$$\rho = \sqrt{x^2 + y^2 + z^2}, \quad (3)$$

$$\phi = \tan^{-1} \frac{y}{x}, \quad (4)$$

$$\theta = \cos^{-1} \frac{z}{\rho}. \quad (5)$$

Here, we set the maximum range of interest to 500 m with a radial step size of 1 m. Future adaptations of this method can vary both the maximum range and step size, depending on the context length of the respective applications. To train a transformer to predict radio propagation behavior, the scene surrounding the BS is interpreted as a collection of unique radio propagation sequences. We then create a range array termed $\delta^{1:R_{\max}}$, containing ascending steps of radius up to a maximum range R_{\max} . Each spatial coordinate is characterized by a distinct $[\phi, \theta]$ 3D angle pair and ρ value, which is binned into a position within $\delta^{1:R_{\max}}$. This representation of unique radio propagation directions enables us to construct REMs with discrete steps along the radial domain while still retaining continuous angular domain information.

B. Transformer based REM Generation

Given a dataset S with N 3D spatial points, for each point $i \in [1, \dots, N]$ with coordinates $[x_i, y_i, z_i]$ and their RSRP values Ω_i , we generate a radio propagation feature sequence Γ_i that encodes the 3D spatial direction. Γ_i is an array of dimension $6 \times R_{\max}$, including $[\log_{10}(\delta^{1:R_{\max}}); \theta_i \times I; \phi_i \times$

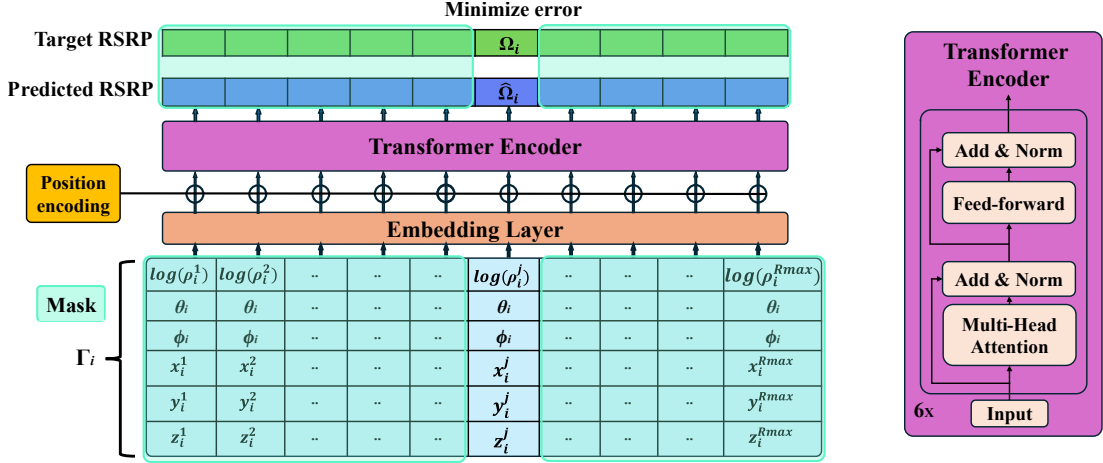


Fig. 3. The masked input feature Γ_i conveys the position information of the i^{th} spatial point, and the transformer encoder is trained to predict its RSRP Ω_i .

$I; x_i^{1:R_{\max}}; y_i^{1:R_{\max}}; z_i^{1:R_{\max}}$, where I is an identity vector of dimension $1 \times R_{\max}$, while $x_i^{1:R_{\max}}$, $y_i^{1:R_{\max}}$, and $z_i^{1:R_{\max}}$ are the cartesian coordinates at every radial bin position along the i^{th} point's angular direction.

The feature vector Γ_i is provided as the input feature to an encoder-only transformer model, as depicted in Fig. 3. The encoder model approach is inspired by the foundational wireless transformer model presented in [15]. The input is parsed through an embedding layer, which extracts higher-dimensional features, followed by a position encoding layer, which incorporates their relative position within the sequence. Next, the transformer encoder comprises 6 attention layers and 8 attention heads within each multi-head attention block. Similar to the training of most transformers and large foundational models, we adopt a two-step approach to learn radio wave propagation behavior. First, we pre-train the model using synthesized signal strength data, which is generated from the FSPL model with its characterized antenna gain pattern while excluding any shadowing components. Subsequently, we fine-tune the model's predictive performance using real-world data. This implicitly allows the model to learn the deviated antenna patterns and shadowing components observed in the data, thereby orienting its predictions closer to each BS site's specific radio propagation environment.

1) **Model-based pre-training (Stage-1):** In this step, we generate the RSRP sequences for every point i in space, along its angular direction ϕ_i, θ_i . The power $P_{b,i_{\text{dB}}}^j$ at each element j along the δ_i^j vector is given by,

$$P_{b,i_{\text{dB}}}^j(\rho_i^j, \phi_i, \theta_i) = P_{b_{\text{dB}}} + \text{FSPL}_{b,i_{\text{dB}}}(\rho_i^j) + A_{\text{dB}}(\phi_i, \theta_i),$$

$$\text{FSPL}_{b,i_{\text{dB}}}(\rho_i^j) = 147.55 - 20 \log_{10}(\rho_i^j) - 20 \log_{10}(f_c), \quad (6)$$

where $P_{b_{\text{dB}}}$ is the BS transmit power, $\text{FSPL}_{b,i_{\text{dB}}}^j$ is the free space path loss value depending on ρ_i^j , the transmit frequency f_c , and finally, the antenna directivity gain through A_{dB} . These synthesized RSRP vectors are the target vectors used to learn the inverse square law of signal strength attenuation. The pre-

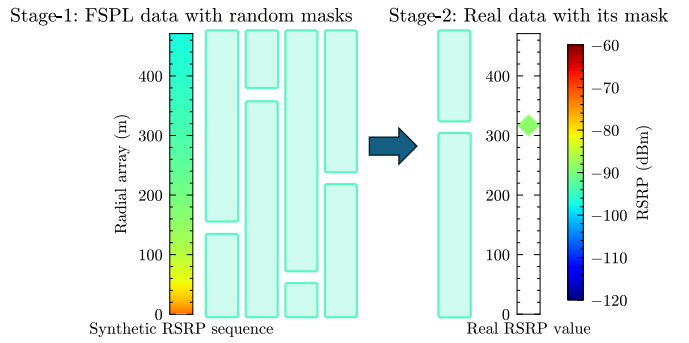


Fig. 4. The feature mask from Fig. 3 is varied by training stage. The pretraining stage leverages complete sequence information by using random masks at each training iteration, and the fine-tuning stage corrects predictions using masks to align with the limited real-world data.

training stage involves masking the input features and the target vector at random positions along the entire sequence length, inspired by [15]. The availability of a continuous sequence of synthetic data in each propagation direction allows random position masking as seen in Fig. 4. The synthetic dataset from surrounding space is used for batch-training with mean square error (MSE) loss function, and a linear warmup and square-root decay (LWSRD) learning rate adaptation algorithm to quickly reach convergence. The pretraining stage prepares the model for fine-tuning at each BS site based on site-specific real-world data.

2) **Data-driven fine-tuning (Stage-2):** In this step, we use real-world data to generate the Γ_i feature vectors. We generate masks to block the portion of the input features, except for the k^{th} column, where k is the bin corresponding to the position of point i in $\delta^{1:R_{\max}}$. The mask dimensions are $6 \times R_{\max} - 1$, and it serves to convey only relevant features of the k^{th} column to the encoder model. The target vector will only contain the real-world RSRP value at the k^{th} position and is used to fine-tune predictions accordingly. The real-world signal

TABLE I
TRANSFORMER ENCODER MODEL TRAINING PARAMETERS.

Parameter	Stage-1	Stage-2
Embedding layer dimension	64	
Number of encoder layers	6	
Number of attention heads	8	
Maximum sequence length	Rmax	
Loss function	MSE	Smooth L1 loss
Learning rate technique	LWSRD	Step decay
Learning rate range	0.0005-0.0001	0.00005-0.00001
Batch size	16	4
Epochs	10	100

strength data points tend to fluctuate drastically due to phase mismatch and noise issues at the receiver. To prevent overfitting to such inconsistencies, we adopt the Smooth L1 loss function, which is robust to large deviations during training. Despite the extensive masking of both input features and outputs necessitated by the limited number of real-world samples, the encoder exhibits robust generalization capabilities.

V. EVALUATION AND RESULTS

In this section, we present the evaluation studies of our two-stage transformer-based REM generation technique. First, we test the accuracy of REM reconstruction using data from [1] after each training stage. With the same dataset, we then compare our results against the Kriging algorithm implementation in [6], treating it as a baseline method. Finally, we use a different dataset from [2] and perform further validation of our method.

A. Two-stage Training Performance

The AERPAW dataset [1] contains 96,000 points in total. We perform a filtering step to remove points reporting RSRP values below -120 dBm, leaving approximately 17,000 points at each altitude. We divide the total data into a train:validate:test split with a 0.75 : 0.05 : 0.2 ratio. These data points are correspondingly translated into their respective Γ_i feature representations. Table I contains the training parameters used for the two-stage training used for this evaluation. Fig. 5 depicts the REM generation against the test set after each training stage, and the quantitative results are recorded in Table II.

This dataset contained a strongly upward-directed antenna beam with increasing energy at higher altitudes of the measurement data. However, this beam pattern was not evident from the provided antenna pattern. As a result, the stage 1 results show weaker signal strength values at higher altitudes, whereas stage 2 fine-tuning refines the REM according to the observations from the dataset. This behavior is observed in the subplots c) vs e) and d) vs f) in Fig. 5. We make use of the root mean square error (RMSE) and mean absolute error (MAE) metrics for a robust evaluation of regression accuracy. We also include the coefficient of determination R^2 , defined as:

$$R^2 = 1 - \frac{\sum_{i=1}^N (\Omega_i - \hat{\Omega}_i)^2}{\sum_{i=1}^N (\Omega_i - \bar{\Omega})^2} \quad (7)$$

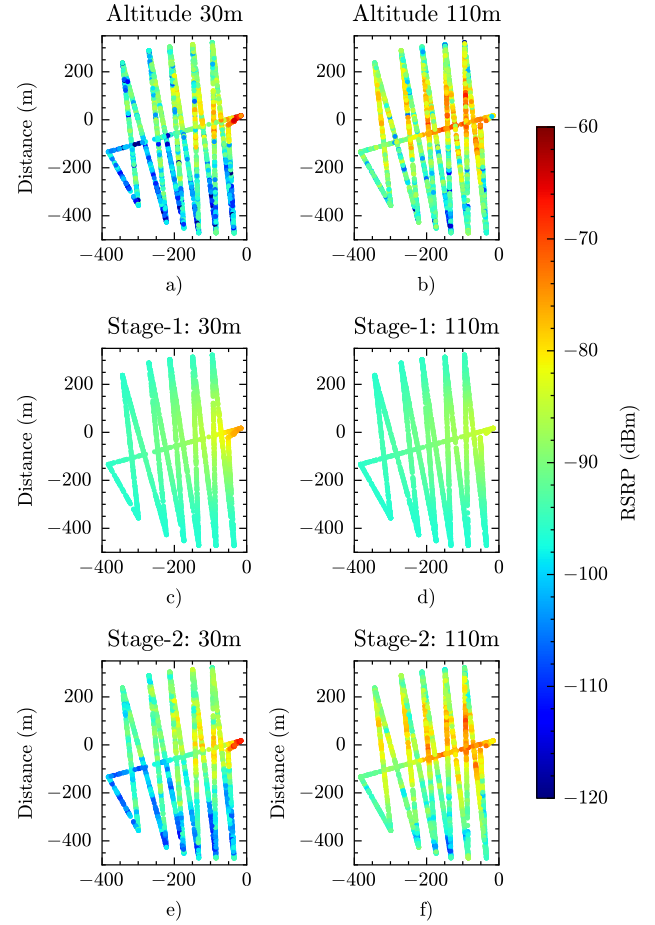


Fig. 5. a) and b) are the test datasets at the lowest and highest altitude. c) and d) are the stage 1 test set predictions learned from FSPL data. Finally, e) and f) are the best fit test predictions after stage 2 fine-tuning.

TABLE II
REM RECONSTRUCTION RESULTS. METRICS FOR TRIPLELAYERML ARE EXTRACTED FROM [2] AS REPORTED THEREIN.

Dataset	REM Method	RMSE	MAE	R^2
AERPAW dataset [1]	TransfoREM Stage 1	7.49 dB	6.20 dB	0.33
	TransfoREM Stage 2	4.57 dB	3.13 dB	0.77
	TransfoREM Stage 1	5.47 dB	3.43 dB	-0.27
	TransfoREM Stage 2	1.29 dB	0.78 dB	0.93
Case Study dataset [2]	TripleLayerML Stage 1	4.07 dB	3.04 dB	0.90
	TripleLayerML Stage 2	1.27 dB	0.82 dB	0.95
	TripleLayerML Stage 3	1.12 dB	0.69 dB	0.95

where Ω_i is the real value, $\hat{\Omega}_i$ is the predicted value, and $\bar{\Omega}$ is the average of all real values, to convey the ability to model the variability in the data. From Table II, we observe that stage 2 fine-tuning achieves improved prediction performance with nearly 3 dB improvement compared to stage 1 in both error metrics and also a desirable increase in R^2 value.

B. Interpolation and Extrapolation between Various Altitudes

To build on the REM effort in [6], using their Kriging technique as the baseline, we evaluate REM generation using data from different altitudes. The transformer model in our approach

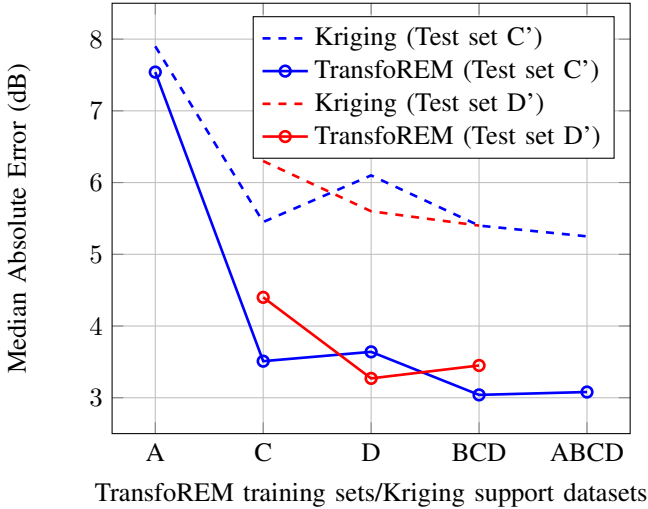


Fig. 6. TranfoREM with signal propagation sequence learning can extrapolate across altitudes better than shadow correlation-based Kriging interpolation.

learns radio propagation patterns from the training data through backpropagation and weight updates. In contrast, the Kriging method utilizes the semivariogram to select highly correlated data points and performs a covariance-based weighted sum of their signal strengths. The transformer is a single-shot estimator for each query point, with an inference computational complexity of $O(N^2)$. On the other hand, the Kriging technique relies on matrix inversion for weight calculation, which leads to a complexity of $O(N^3)$. Overall, the transformer-based technique is well-suited for batch inference and network deployment. We borrow the median average error results from [6] and compare the estimation performance between the two techniques. Following a similar evaluation procedure, we label the data from various altitudes as A: 50 m, B: 70 m, C: 90 m, D: 110 m, and test both 2D and 3D extrapolation properties by learning from various dataset combinations and testing on disjoint subsets C': 90 m and D': 110 m. Fig. 6 depicts the improved REM inference performance of TranfoREM against the kriging technique, with an average improvement of 1.5 dB.

C. Case Study: Cascaded TripleLayerML architecture

The authors of [2] have meticulously collected Long Term Evolution (LTE) KPIs from a BS using a UAV. This published dataset has been filtered to remove outliers and partitioned into 8881 training points and 2144 testing points. We utilize this dataset and provide a comparative evaluation against their triple-layer ML approach. The TripleLayerML approach estimates the KPIs, and corrects for errors with a new ML model at each stage. The results in Table II indicate the stage-wise improvement in performance, reaching very low RMSE and MAE values. While this approach provides a low REM reconstruction error, training three different ML techniques for each BS site is more complex, with the third GPR layer having $O(N^3)$ complexity. The TripleLayerML method also reports a latency-optimized variant that exhibits worse performance,

indicating a tradeoff between complexity and accuracy. From Table II, we observe that TransfoREM performs identically to the TripleLayerML after Stage 2. Our approach is also less complex and ready to be deployed at each BS for continual online REM fine-tuning.

VI. CONCLUSION

We frame REM generation as a physics-aligned sequence estimation problem and propose a novel two-stage hybrid training approach for a masked Transformer model. This method effectively utilizes limited real-world data, demonstrating superior accuracy in REM construction compared to other techniques. Finally, TransfoREM can be seamlessly integrated into REM frameworks in wireless networks to enable the online learning of spatial radio propagation information, which can then be used for informed network management decisions.

REFERENCES

- [1] S. J. Maeng, O. Ozdemir, I. Guvenc, and M. L. Sichitiu, "Kriging-Based 3-D Spectrum Awareness for Radio Dynamic Zones Using Aerial Spectrum Sensors," *IEEE Sensors J.*, vol. 24, no. 6, pp. 9044–9058, 2024.
- [2] H. A. H. Alobaidy, M. Behjati, R. Nordin, M. A. Zulkifley, N. F. Abdulla, and N. F. M. Salleh, "Empirical 3D Channel Modeling for Cellular-Connected UAVs: A Triple-Layer Machine Learning Approach," 2025. [Online]. Available: <https://arxiv.org/abs/2505.19478>
- [3] S. Bi, J. Lyu, Z. Ding, and R. Zhang, "Engineering Radio Maps for Wireless Resource Management," *IEEE Wireless Commun.*, vol. 26, no. 2, pp. 133–141, 2019.
- [4] S. Zhang and R. Zhang, "Radio Map-Based 3D Path Planning for Cellular-Connected UAV," *IEEE Trans. on Wireless Commun.*, vol. 20, no. 3, pp. 1975–1989, 2021.
- [5] D. Romero and S.-J. Kim, "Radio Map Estimation: A data-driven approach to spectrum cartography," *IEEE Signal Process. Mag.*, vol. 39, no. 6, pp. 53–72, 2022.
- [6] M. Rahman, S. J. Maeng, I. Guvenc, and C.-W. Wong, "3D Spectrum Awareness for Radio Dynamic Zones Using Kriging and Matrix Completion," in *IEEE Int. Symposium on Dynamic Spectrum Access Networks (DySPAN)*, 2024, pp. 439–446.
- [7] B. Feng, M. Zheng, W. Liang, and L. Zhang, "A Recent Survey on Radio Map Estimation Methods for Wireless Networks," *Electronics*, vol. 14, no. 8, p. 1564, 2025.
- [8] R. Shrestha, T. N. Ha, P. Q. Viet, and D. Romero, "Radio Map Estimation in the Real-World: Empirical Validation and Analysis," in *IEEE Conf. on Antenna Measurements and Applications (CAMA)*, 2023, pp. 169–174.
- [9] R. Shrestha, D. Romero, and S. P. Chepuri, "Spectrum Surveying: Active Radio Map Estimation With Autonomous UAVs," *IEEE Trans. on Wireless Commun.*, vol. 22, no. 1, pp. 627–641, 2023.
- [10] K. Yin, S. Fang, F. Chu, and Y. Fan, "Compressed Tensor Completion: Approach for UAV-Aided 3-D Radio Map Construction," *IEEE Internet of Things J.*, vol. 11, no. 24, pp. 40 516–40 531, 2024.
- [11] X. Li, S. Zhang, H. Li, X. Li, L. Xu, H. Xu, H. Mei, G. Zhu, N. Qi, and M. Xiao, "RadioGAT: A Joint Model-Based and Data-Driven Framework for Multi-Band Radiomap Reconstruction via Graph Attention Networks," *IEEE Trans. on Wireless Commun.*, vol. 23, no. 11, pp. 17 777–17 792, 2024.
- [12] T. Hu, Y. Huang, J. Chen, Q. Wu, and Z. Gong, "3D Radio Map Reconstruction Based on Generative Adversarial Networks Under Constrained Aircraft Trajectories," *IEEE Trans. on Veh. Technol.*, vol. 72, no. 6, pp. 8250–8255, 2023.
- [13] P. Q. Viet and D. Romero, "Spatial Transformers for Radio Map Estimation," in *IEEE Int. Conf. on Commun.*, 2025, pp. 6155–6160.
- [14] M. Benzaghta, G. Geraci, D. López-Pérez, and A. Valcarce, "Cellular Network Design for UAV Corridors via Data-driven High-dimensional Bayesian Optimization," *IEEE Trans. on Wireless Commun.*, pp. 1–1, 2025.
- [15] S. Alikhani, G. Charan, and A. Alkhateeb, "Large Wireless Model (LWM): A Foundation Model for Wireless Channels," 2025. [Online]. Available: <https://arxiv.org/abs/2411.08872>